A local ATR-dependent checkpoint pathway is activated by a site-specific replication fork block in human cells.

Sana Ahmed-Seghir[2,4], Manisha Jalan[2,4], Helen E. Grimsley[2], Aman Sharma[2], Shyam Twayana[3], Settapong T Kosiyatrakul[3], Christopher Thompson[2], Carl L. Schildkraut[3, *], Simon N. Powell[1,2,*]

[1]Molecular Biology Program, Memorial Sloan Kettering Cancer Center, New York, New York, USA.

[2]Department of Radiation Oncology, Memorial Sloan Kettering Cancer Center, New York, New York, USA.

[3]Department of Cell Biology, Albert Einstein College of Medicine, Bronx, NY 10461

[4]These authors contributed equally: Sana Ahmed-Seghir and Manisha Jalan

[*]Co-corresponding Authors

email: powells@mskcc.org; carl.schildkraut@einsteinmed.edu

Keywords: DNA damage; DNA repair; DNA replication; genomic integrity; genomic instability; replication stress; ATR

Abstract

When replication forks encounter DNA lesions that cause polymerase stalling a checkpoint pathway is activated. The ATR-dependent intra-S checkpoint pathway mediates detection and processing of sites of replication fork stalling to maintain genomic integrity. Several factors involved in the global checkpoint pathway have been identified, but the response to a single replication fork barrier (RFB) is poorly understood. We utilized the *E.coli*-based Tus-*Ter* system in human MCF7 cells and showed that the Tus protein binding to *TerB* sequences creates an efficient site-specific RFB. The single fork RFB was sufficient to activate a local, but not global, ATR-dependent checkpoint response that leads to phosphorylation and accumulation of DNA damage sensor protein γH2AX, confined locally to within a kilobase of the site of stalling. These data support a model of local management of fork stalling, which allows global replication at sites other than the RFB to continue to progress without delay.

38 ## Introduction

39 Genomic DNA is constantly exposed to exogenous and endogenous damaging agents,
40 forming DNA lesions that challenge the progression of replication forks (RFs) during the
41 S-phase of the cell cycle. The genome contains natural impediments, which cause
42 replication stalling such as common fragile sites, repeated sequences, non-B structures,
43 sites of collision between transcription and replication machinery, or DNA-protein
44 complexes (Mirkin and Mirkin, 2007). These replication fork barriers (RFB) can impede
45 the progression of the replication machinery and if unresolved, lead to genomic
46 instability, a common hallmark of aneuploidy, neurological and neuromuscular
47 disorders, and cancer.

48 Replication stress can impede the progression of the replication fork. During
49 replication stress, the intra-S phase checkpoint pathway can be activated at a local and
50 global level which is a critical step to process the DNA lesions and maintaining genome
51 integrity. The S-phase checkpoint involves the uncoupling of replicative polymerases
52 from the replicative helicase and the generation of ssDNA, which rapidly gets coated
53 with RPA. In turn, this activates ATR/ATRIP kinase signaling with its effector kinase
54 CHK1, plus phosphorylation of H2AX at Ser139 in response to a variety of lesions which
55 promote cell cycle arrest, fork stabilization, and restart (Iyer and Rhind, 2017, 2013;
56 Willis and Rhind, 2009a; Zeman and Cimprich, 2013).

57 Previous studies suggest that the local and global intra-S checkpoints are two
58 distinct mechanisms that can be distinguished by the signaling intensity of detecting
59 DNA damage (Saxena and Zou, 2022). It is thought that a threshold of DNA damage
60 must be reached to activate the global checkpoint and impact cell cycle progression
61 during replication (Bantele et al., 2019; Shimada et al., 2002). The local checkpoint
62 reacts to a unique replication fork stalling site, which does not impact overall cell cycle
63 progression. The proteins involved in the global replication stress response have been
64 identified using DNA damaging agents that lead to multiple DNA lesion formation
65 randomly throughout the genome. Nevertheless, the mechanism and timing of the
66 checkpoint pathway at a local scale remain largely unknown and are critical to
67 understanding the series of processes at a single RF stall.

68 In the *E.coli* genome, the DNA pausing sequences called terminator (Ter) are
69 recognized by a protein called Tus to cause a polar site-specific arrest of the RF at the
70 end of the bacterial chromosome replication (Hiasa and Marians, 1994; Hidaka et al.,
71 1988; Mulcair et al., 2006; Roecklein et al., 1991). The Tus-*Ter* complex leads to a
72 temporarily locked complex on DNA that can be overcome by the fork arriving in the
73 opposite direction, displacing Tus to terminate replication. The artificial *E.coli*-based
74 Tus/Ter system has previously been employed in mouse embryonic stem cells to
75 measure homologous recombination repair products and investigate the DNA repair
76 pathway choice (Chandramouly et al., 2013; Willis et al., 2017, 2014).

77 In this study, we integrated a plasmid with 5 repeats of the *TerB* sequence in the
78 non-permissive orientation at a unique site within chromosome 12 of the breast cancer
79 cell line MCF7 (MCF7 5C-TerB clone). We utilized the integrated Tus-*TerB* system in
80 human MCF7 cells to artificially generate individual RFBs and investigated the
81 activation of the S-phase checkpoint signaling mechanism. We show that Tus/Ter
82 creates an efficient site-specific RFB in human cells and observed local activation of
83 ATR signaling which was responsible for the phosphorylation of DNA damage marker
84 γH2AX at the stall sites. When a replication fork pauses at the local Tus-*TerB* block, we
85 do not detect any alteration in global replication profiles. Our system allows us to study
86 the ATR-checkpoint activity as a local response to a single RFB.

87

88 Results

89 Tus is found enriched at *TerB* sites integrated in human cells

90 The 23 bp *TerB* sequence in interaction with the Tus protein have been successfully
91 used in yeast and mice to create artificial RFBs (Larsen et al., 2014a, 2014b; Willis et
92 al., 2018, 2017, 2014; Willis and Scully, 2016). To study the effect of site-specific
93 replication blocks at a genomic locus in human cells, a previously established MCF7
94 clone with a unique integrated copy of a plasmid carrying two sets of 5 repeats of the
95 *TerB* sequence in the non-permissive orientation was used (Fig.1A, SupFig1). Whole
96 genome sequencing of the clone was carried out to confirm the single copy integration

97 of the plasmid at hg38 chr12:95325001. Firstly, we checked if Tus protein was able to
98 bind *TerB sequences* in this artificial system in human cells. Chromatin-
99 Immunoprecipitation (ChIP) followed by quantitative Polymerase Chain Reaction
100 (qPCR) was performed using an antibody against the His-tag 24h after MCF7 5C-TerB
101 cells were transfected with a Tus-His expression plasmid. The Tus signal is specifically
102 enriched over 20 times compared to the vector control (VC) condition in proximity to the
103 *TerB* sequences (PP9, 2, and 47) (Fig.1B).

104 To corroborate this observation, we performed the proximity ligation assay (PLA)
105 (see methods). Two tagged-Tus (HA-Tus and Tus-His) or a VC expression plasmid
106 were simultaneously transfected and antibodies against the two tags, HA and His, were
107 used to generate a PLA signal (Fig.1C, D). We observed 19% of the cells transfected
108 with the two tagged Tus were harboring one or two PLA signal versus 9% of the cells
109 transfected with the VC (Fig.1E), a significant enrichment of the PLA signal when Tus
110 was bound to *TerB*. These results indicate a specific interaction of the Tus protein with
111 the *TerB* sequences in human cells.

112 **The Tus-*TerB* barrier is an efficient block to incoming replication forks**

113 It has previously been demonstrated that the Tus-*TerB* interaction can induce an RFB in
114 mouse embryonic cells in an episomal system (Willis et al., 2014). We reasoned that
115 our integrated system in MCF7 cells would be more prone to replication fork arrests
116 near the *TerB* sequences. We used single-molecule analysis of replicated DNA
117 (SMARD) to investigate evidence of replication fork stalling in the genomic DNA (Norio
118 and Schildkraut, 2001). The self-labeling SNAP-tag was used to label Tus. After
119 induction of Myc-NLS-TUS-SNAP by using Dox for 3 days, asynchronous MCF7 5C-
120 TerB cells were sequentially pulse-labeled using two nucleoside analogs
121 (iododeoxyuridine (IdU) and chlorodeoxyuridine (CldU)) for 4h each (Fig.2A). The
122 isolated DNA was digested by restriction endonuclease SfiI and the 200 kb fragment
123 obtained was stretched on slides for staining. Two DNA FISH probes were used to
124 detect the 200 kb segment of interest containing the *TerB* arrays: one probe of 40 kb
125 within the chromosome 12 (hg38 chr12:95,199,827 – 95,239,226) and one probe of 7
126 kb made from pWB15 (Fig.2B). The direction of replication forks could be determined

127 using the labeling patterns and its position within the locus of interest using our FISH
128 probes. After inducing the expression of Myc-NLS-TUS-SNAP from an integrated
129 plasmid in MCF7 5C-TerB cells (SupFig.2A, B), we analyzed its impact on the
130 replication fork progression within the region containing *TerB* repeats (Fig.2C, D). The
131 yellow arrows indicate the transition of labeling from IdU to CldU incorporation showing
132 the replication fork direction. When Tus was expressed, these transition sites were
133 found accumulated near the *TerB* regions (Fig.2D, arrows within the white oval)
134 compared to the random signal spread on the 200 kb region when Tus is not expressed
135 (Fig.2C). We quantified the percentage of molecules with replication forks at each 5 Kb
136 interval in the 200 kb SfiI segment containing *TerB* sequences (Fig.2E, F) and
137 confirmed an accumulation of forks at the *TerB* sequences only when Tus was
138 expressed (Fig.2F, black arrow) supporting that the binding of Tus on *TerB* arrays can
139 impair the replisome progression at genomic loci. Interestingly, expression of the Tus
140 protein alone does not alter the direction of replication fork progression along the 200 kb
141 SfiI segment where forks predominantly progress from the 3' to 5' direction in cells both
142 with and without Tus expression as analyzed by the percentage of molecules with IdU
143 incorporation at each 5 kb interval (SupFig.2C, D). Furthermore, no significant difference
144 was observed in the global replication fork speed in cells with or without Tus expression
145 (SupTable1). Together, these data indicate that when Tus bound the *TerB* sequences
146 integrated within chromosome 12, it creates a physical barrier and an obstacle to the
147 replication fork progression.

148 The eukaryotic replisome is a multiprotein apparatus consisting of DNA
149 helicases, DNA polymerases and accessory proteins to duplicate the genome. We
150 hypothesized that an RFB would induce an accumulation of these proteins on chromatin
151 around *TerB* sequences. To test our hypothesis, we performed ChIP using an antibody
152 against mini-chromosome maintenance protein 3 (MCM3), a CMG core-complex
153 protein, in the absence or presence of Tus. When Tus was expressed, MCM3 was 3-
154 fold more enriched upstream of the *TerB* arrays at the PP0-2 and PP10 sites compared
155 to the surrounding primer pairs (Fig.2G, H). Additionally, we find that there is an
156 enrichment of the DNA repair scaffold protein FANCM at the *TerB* sites mirroring the
157 MCM3 enrichment (SupFig.3), indicative of the stalled replication forks as previously

158 described (Collis et al., 2008; Nandi and Whitby, 2012; Panday et al., 2021; Xue et al.,
159 2015). Together, these results show that Tus expression induces a RFB at the *TerB*
160 arrays impairing the replisome progression during S-phase.

161 **γH2AX is enriched at *TerB* sites after Tus expression before fork collapse**

162 One of the earliest responses to replication stress is the phosphorylation of the histone
163 variant H2AX on serine 139 (γH2AX) by members of the phosphoinositide 3-kinase
164 (PI3K)-like family (PIKK) (Ward and Chen, 2001). As we demonstrated that *TerB* arrays
165 can block incoming replication forks, we asked whether we could see a γH2AX signal
166 enrichment due to fork arrest. Using a co-immunoprecipitation assay with the chromatin
167 fraction of cross-linked-cells expressing either GFP tag or GFP-Tus, we found that GFP-
168 Tus and γH2AX were immunoprecipitated together using GFP or γH2AX antibodies
169 (Fig.3A).

170 To gain insight into the γH2AX signal at the RFB induced by the Tus-*TerB*
171 interaction, cells were transfected with either VC or HA-Tus expression plasmids, and
172 PLA was performed using antibodies against HA and γH2AX (Fig.3B). We found that
173 16% of the HA-Tus transfected cells were harboring at least one PLA signal versus 3%
174 of the VC transfected cells (Fig.3C).

175 To better characterize the γH2AX enrichment around *TerB* sites, we performed
176 ChIP-qPCR assays using a γH2AX antibody 24h after Tus or VC expression. We
177 observed an enrichment of γH2AX, strictly co-localizing with the Tus-Ter interaction
178 sites (PP9 and PP47), suggesting a local role of γH2AX in response to stalled RFs
179 (Fig.3D, E). This is in stark contrast to the observed spreading of the γH2AX signal after
180 a site-directed DSB (Berkovich et al., 2007; Chailleux et al., 2014; Clouaire et al., 2018;
181 Savic et al., 2009). To corroborate this observation in our integrated cassette, we
182 generated a site-specific DSB by expressing Cas9 targeted to the integrated cassette
183 (SupFig.4A-C). We assessed γH2AX using the ChIP-qPCR assay 24h after transfection
184 and noticed enrichment at the distal primer pair (PP10) contrasting with the very tight
185 local signal observed at the Tus-*TerB* RFB (SupFig.4D). However, we did not find any
186 significant γH2AX signal between VC or Tus expression (SupFig 5A-B) supporting the
187 lack of global response. This suggests that the RFB generated by the interaction

188 between Tus and the *TerB* arrays activates a stress response that stimulates the
189 phosphorylation of H2AX, concentrated around the fork block.

190 **H2AX is phosphorylated in an ATR-dependent manner without a global activation**
191 **of the intra-S checkpoint**

192 ATR is known to phosphorylate H2AX in response to replication stress and plays a
193 pivotal role in the surveillance of DNA replication (Ward and Chen, 2001). To
194 understand if the global ATR-dependent checkpoint was activated in response to the
195 Tus-*TerB* RFB, we analyzed the levels of phospho-proteins involved in the intra-S
196 checkpoint activation pathway (RPA, CHK1, and ATR) by immunoblotting fractionated
197 cell extracts 24h after VC or Tus expression. Cells treated with 2mM hydroxyurea (HU)
198 for 4h demonstrated an increase in phospho-protein levels, acting as a control for
199 checkpoint activation (Fig 4.A, lanes 3 and 4). Tus expression alone did not activate the
200 global ATR-dependent checkpoint as the level of phospho-protein remained the same
201 as the VC control (Fig 4.A, lanes 1 and 2). We did not find any observable difference in
202 cell cycle progression between VC or Tus expression alone (SupFig6 A-B) supporting
203 the lack of global response.

204 We hypothesized that if the local γH2AX enrichment at *TerB* sites was ATR-
205 dependent, a reduction of ATR activity would lead to a decreased γH2AX signal. To
206 validate the ATR inhibitor activity (ATRi), VE-822 (Fokas et al., 2012), we performed
207 immunoblotting using total protein extracts of cells treated with 2mM HU and compared
208 the level of phospho-ATR TH1989 with or without an ATR inhibitor. A 4h treatment with
209 ATRi reduced the level of phospho-ATR TH1989, reflecting a decrease in ATR activity
210 (Fig.4B). ChIP-qPCR assays were performed using a γH2AX antibody 24h after VC or
211 Tus expression and cells were harvested after a 4h ATRi treatment. Consistent with our
212 hypothesis, the γH2AX enrichment in the vicinity of *TerB* sites after Tus expression was
213 remarkably decreased upon ATRi treatment (Fig.4C PP9 and PP47), implying that the
214 Tus-*TerB* RFB activates a localized stress response that stimulated the local
215 phosphorylation of H2AX. Together, these data suggest a local activation of the intra-S
216 checkpoint via the ATR kinase and rapid phosphorylation of H2AX, which could mediate
217 the recruitment of repair factors near the damage site.

218 ## Discussion

219 Replication stress occurs during the S-phase of the cell cycle, when the replication
220 machinery encounters DNA lesions that cause stalling of replicative polymerases and
221 can be a significant cause of genomic instability. If the stalled forks cannot be
222 processed, they can result in DNA breakage, mutations, and chromosomal
223 rearrangements leading to the development of many different human cancers (Gaillard
224 et al., 2015; Tubbs and Nussenzweig, 2017). In this study, we used the reconstituted
225 *E.coli*-derived protein-DNA barrier, Tus-*TerB,* to study the replication stress response at
226 a single RFB. We have shown that the Tus protein efficiently binds at the *TerB*
227 sequences using ChIP-qPCR and PLA in MCF7 cells (Fig.1). We confirmed that this
228 integrated system was able to cause site-specific RFB at *TerB* sequences when Tus
229 was introduced with the use of the SMARD technique and observed the accumulation of
230 replication fork protein MCM3 upstream of *TerB* sequences (Fig.2). Our results indicate
231 that the integrated Tus-*TerB* system acts as an efficient site-specific replication fork
232 barrier, providing valuable insights into the local processing of a stalled single fork in
233 human cells and its difference from global replication stress (Fig.5).

234 We show that the site-specific replication stress leads to the accumulation of
235 γH2AX at the site of fork block when Tus was expressed by co-immunoprecipitation of
236 Tus and γH2AX (Fig.3A). Additionally, we confirmed that γH2AX is localized at the site
237 of Tus-*TerB* using PLA and ChIP-qPCR assays (Fig.3B,C). We suggest that the γH2AX
238 signal is being constrained to a region of less than a kilobase from the *TerB* sites by
239 tortional stress generated when the replication fork encounters the barrier and is not
240 influenced by well-defined topological domains that are one measure of the functional
241 units of the genome (Dixon et al., 2012; Rao et al., 2014). Furthermore, there was no
242 observable difference in global replication profiles or the activation of global checkpoint
243 markers such as pRPA, pCHK1, and pATR, with or without Tus protein expression,
244 contrasting with the differences observed in the presence and absence of HU-induced
245 replication stress (Fig.4A, SupTable1 & SupFig.5,6). We conclude that Tus-*TerB*-
246 induced replication fork stall does not activate global ATR-dependent S-phase
247 checkpoint signaling, suggesting that a local response is occurring at the stalled

248 replication fork. Interestingly, upon ATR inhibition, we observed that the enrichment of
249 phosphorylated H2AX at *TerB* sites was significantly reduced when Tus was expressed,
250 which indicates local ATR signaling is responsible for the phosphorylation of H2AX at
251 the stalled site (Fig.4C,D). This localized ATR-dependent γH2AX differs from the well-
252 observed ATM-dependent spreading of γH2AX signal after a site-directed double-strand
253 break (Berkovich et al., 2007; Chailleux et al., 2014; Clouaire et al., 2018; Savic et al.,
254 2009) and suggests a distinct local intra-S phase checkpoint is being activated in
255 response to the single RFB.

256 There are additional mechanisms to be understood in this newly described local
257 replication stress response, which includes whether the activation of ATR is dependent
258 on ATRIP. ATRIP requires binding to ssDNA, but in unpublished observations we have
259 not found significant ssDNA (using RPA-ChIP) in response to Tus-TerB replication
260 stalling. In the Tus-*TerB* system, there is no known dissociation of the replicative
261 helicase from the polymerase, which is responsible for the ssDNA signal. Therefore, just
262 like ATM can be activated independently of the MRE11 complex (Bakkenist and Kastan,
263 2003), we expect that ATR is activated independently of ATRIP, likely due to local
264 changes in chromatin that will be investigated in future studies.

265 During extensive DNA damage, the genome-wide checkpoint response activates
266 ATR/CHK1 globally, which leads to the slowing of all replication forks in the cell,
267 inhibition of cell cycle progression, and suppression of late origin firing; to provide
268 sufficient time for DNA repair. It has been proposed that a local checkpoint response
269 occurs when one or a few replication forks encounter a DNA lesion and activates
270 ATR/CHK1 signaling at local sites of fork stalling. The local ATR response has been
271 hypothesized to be transient, in which the fork moves slowly only at stalled sites to
272 promote fork stabilization, restart the stalled fork, and suppress recombination without
273 triggering the global checkpoint response (Iyer and Rhind, 2017, 2013; Kaufmann et al.,
274 1980; Merrick et al., 2004; Saxena and Zou, 2022; Willis and Rhind, 2009b; Zeman and
275 Cimprich, 2013).

276 We predict that the local ATR-dependent checkpoint signaling can result in a
277 rapid and controlled response to allow RFB resolution, through the recruitment of repair

278 factors to the damaged site. The factors might include those involved in fork
279 stabilization, fork reversal, fork cleavage, and homology-dependent replication restart
280 (Saxena and Zou, 2022). The Tus-*TerB* system has previously been employed in
281 mouse embryonic stem cells to measure and investigate the DNA repair pathway choice
282 (Chandramouly et al., 2013; Panday et al., 2021; Willis et al., 2017, 2014). This included
283 both error-free and error-prone homologous recombination induced by a mammalian
284 chromosomal RFB, as well as identifying the role of the structure-specific endonuclease
285 complex SLX4-XPF and FANCM in the repair of microhomology-mediated tandem
286 duplications that occur at replication arrest (Elango et al., 2022; Nandi and Whitby,
287 2012; Willis et al., 2017). The Tus-*TerB* block is robust and is not dissociated by the
288 action of DNA helicases such as PIF1, corroborated in previous yeast studies that have
289 demonstrated that the "sweepase" RRM3 is unable to resolve this RFB (Larsen et al.,
290 2014b). Therefore, it is likely that the RFB is resolved either by incoming replication
291 forks leading to termination at the *TerB* site or by fork cleavage (Larsen et al., 2014b;
292 Willis et al., 2014). Unpublished work from our laboratory has demonstrated that
293 replication forks are cleaved at or near the *TerB* site, resulting in fork breakage at the
294 barrier. Fork reversal at the Tus-*TerB* site has been observed in the yeast system
295 (Larsen et al., 2014b; Marie and Symington, 2022), but not for the mammalian systems,
296 and it is unlikely that shifting the position of the RFB would make it easier to resolve.
297 Therefore, fork cleavage is the most likely mechanism for resolving the RFB.

298 The upstream pathway of activation of the DNA damage response, as a result of
299 a single RFB, is not completely understood. Previous work has shown that FANCM acts
300 as a scaffolding protein for recruitment of different repair protein complexes involved in
301 the stalled replication fork rescue (Panday et al., 2021; Willis et al., 2017). We observed
302 that the FANCM protein is enriched at the site of the RFB induced by Tus-*TerB*
303 (SupFig.3), confirming a similar phenomenon observed in mouse cells. However, it is
304 yet to be determined if FANCM recruitment to the RFB precedes local H2AX
305 phosphorylation by ATR, or if FANCM is recruited as a consequence of the γH2AX
306 signal to help elicit the downstream DNA damage response (DDR). We also anticipate
307 that the protein complex, 9-1-1 (RAD9A, HUS1, RAD1), and the subsequently recruited

308 TOPBP1, may also play a role at this local ATR-dependent intra-S checkpoint (Helt et
309 al., 2005; Parrilla-Castellar et al., 2004).

310 While the Tus-*TerB* system is an important tool in deciphering signaling at
311 individual replication forks, it will be important to test if the local-S phase model remains
312 supported when exploring endogenous lesions that occur when replication forks
313 encounter secondary structures such as R-loops, G-quadruplexes and common fragile
314 sites characterized by trinucleotide repeat expansion [$(CAG)_n$/$(CTG)_n$] (Brickner et al.,
315 2022; Bryan, 2019; Kim et al., 2016). Here the mechanisms surrounding the
316 identification and resolution of the RFB may differ. Overall, our results indicate that Tus-
317 *TerB* system acts as an efficient RFB and activates local ATR checkpoint signaling at
318 the stall site, leading to phosphorylation and accumulation of the DNA damage sensor
319 protein γH2AX, which is dependent on the ATR kinase. The local γH2AX accumulation
320 at the stalled region would lead to the recruitment of DNA repair factors for resolution of
321 the fork (Fig.5). Together, our findings reveal the signaling mechanism of the Tus/*TerB*
322 induced replication block and showed that the site-specific fork block is dependent on
323 the local ATR S-phase checkpoint signaling.

324

325

326 ## Methods

327 **Cell culture and transfection conditions**

328 MCF7 5C-TerB cells were grown at 37˚C and 5% CO_2 in complete DMEM high glucose
329 supplemented with 10% FBS, 2 mM Glutamax, 20 mM HEPES, 100 I.U./ml Penicillin,
330 and 100 µg/ml Streptomycin supplemented with 400 µg/ml zeocin.

331 For PLA, cells were seeded at $1X10^5$ in a 12-well cell culture plate. For T7 assay, cells
332 were seeded at $2.5X10^5$ in a 6-well cell culture plate. For ChIP, IP and cellular
333 fractionation, cells were seeded at $2.5X10^5$ in a 10 cm cell culture dish.

334 MCF7 5C-TerB cells were seeded and transfected the day after with 10 µg of
335 pCMV3xnls Tus or pCMV3xnls using the Mirus Bio™ TransIT™-LT1 reagents for 24h

336 more. For the generation of DSB, cells were transfected 6h prior harvesting with 120
337 pmol of the sgRNA TerB1 and 120pmol of the Cas9 protein (obtained from QB3
338 Macrolab, Berkeley) using the Lipofectamine CRISPRMAX™ Cas9 transfection
339 reagents.

340 **Generation of stable cell lines**

341 PvuI linearized pWB15 was transfected into MCF7 cells to generate the stably
342 integrated clone, MCF7 5C-TerB (Supplementary Figure 1). 800 µg/ml of Zeocin was
343 used to select positively integrated cells and monoclonal colonies were isolated and
344 subsequently maintained in 400 µg/ml Zeocin. Single integrant validation was performed
345 by whole genome sequencing of the clone.

346 Stable MCF7 5C-TerB cells inducible expressing Myc-NLS-TUS-SNAP were generated
347 by lentiviral transduction. Cells were infected with lentiviral particles containing
348 pInducer10L or pInd Tus-SNAP and single-cell clonal colonies were selected in
349 complete DMEM containing 1 µg/mL puromycin and 400 µg/ml zeocin. Myc-NLS-TUS-
350 SNAP protein was expressed in stable lines by induction with 1 µg/ml doxycycline for 3
351 days.

352 **Plasmid construction**

353 The doxycycline-inducible lentiviral plasmid used to express N-terminally myc-tagged,
354 C-terminally SNAP-tagged nuclear localized, human codon-optimized wild-type Tus
355 (Myc-NLS-TUS-SNAP) was generated as follows. The N-terminally myc epitope-tagged,
356 nuclear-localized, codon-optimized wild-type Tus cDNA sequence was PCR amplified
357 from pcDNA3-β-MYC-NLS-Tus using primers Forward 5'-
358 AGTCGGTACCGAATTCGCCACCATGGAACAAAAGCTG-3' and Reverse 5'-
359 AGTCGGCGGCCGCGCCGCTACCGTCAGCCACGTACAGGTGCA and the SNAP-tag
360 cDNA sequence PCR amplified using primers Forward 5'-
361 AGTCGCGGCCGCCGGCCACATGGACAAAGACTGCGAAATGAAGC-3' and Reverse
362 5'-ACTGCTCGAGTCAACCCAGCCCAGGCTTGC-3'. The Tus and SNAP PCR
363 amplified fragments were digested with KpnI and NotI, and NotI and XhoI, respectively,
364 and inserted into the inducible expression lentiviral vector pInducer10L (Drosopoulos et

365 al., 2020) directly downstream of the doxycycline-inducible promoter, to generate pInd
366 Tus-SNAP. This construct was sequenced to confirm that unintended mutations were
367 not introduced during PCR and cloning.

368 **Immunoblotting**

369 Cells were harvested by trypsinization, suspended in complete DMEM, washed with
370 PBS, then pelleted and flash frozen in liquid N_2 and stored at -80˚C. For SDS-PAGE,
371 pellets were thawed on ice and lysed by resuspending in Laemmli Buffer (60 mM Tris-
372 HCl pH 6.8, 400 mM 2-mercaptoethanol, 2% SDS, 10% glycerol, 0.01% bromophenol
373 blue) to a final concentration of 10^6 cells/ml. Lysates were denatured (5 min at100˚C)
374 and passed through a 25-gauge needle (5x) then spun for 2 min at full speed in a
375 microfuge. Aliquots of lysate corresponding to 10^5 cells were resolved on 4-15%
376 gradient SDS-PAGE gels, proteins transferred to nitrocellulose membrane and blocked
377 in PBS with 5% Blotting-grade Blocker and 0.1% Tween 20. Membranes were then
378 incubated with primary antibodies diluted in PBS with 5% Blotting-grade Blocker.
379 Primary antibodies used were anti-Myc tag and anti-actin. Following incubation with
380 primary antibodies, membranes were washed with PBS + 0.1% Tween 20. Membranes
381 were then incubated with fluorescently labeled Goat Anti-Mouse IRDye 680LT and Goat
382 Anti-Rabbit IRDye800CW secondary antibodies and then washed in PBS + 0.1% Tween
383 20. Immunoblots were imaged on an Odyssey Lc Infrared scanner.

384 **Single Molecule Analysis of Replicated DNA (SMARD) assay**

385 SMARD was performed essentially as previously described (Drosopoulos et al., 2012;
386 Norio and Schildkraut, 2001; Twayana et al., 2021). Exponentially growing cells in
387 complete DMEM with 1 µg/ml doxycycline were sequentially pulse-labeled with IdU (4 h)
388 followed by CldU (4 h) each to a final concentration of 30 µM. Following pulsing, cells
389 were suspended in PBS at a concentration of 3 x 10^7 cells per ml. An equal volume of
390 1% molten TopVision low melting point agarose) in PBS was added. The resulting cell
391 suspension in 0.5% TopVision agarose was poured into wells of a chilled plastic mold to
392 make plugs of size 0.5 cm x 0.2 cm x 0.9 cm, each containing 10^6 cells. Cells in the
393 plug were lysed at 50°C in a buffer containing 1% n-lauroylsarcosine, 0.5 M EDTA, and

394 0.2 mg/ml proteinase K. Plugs were rinsed in TE and washed with 200 μM
395 phenylmethanesulfonyl fluoride (PMSF). Genomic DNA in the plugs was digested with
396 *SfiI* overnight at 37°C. Digested genomic DNA was cast into 0.7% SeaPlaque GTG
397 agarose gel and DNA was separated by pulsed field gel electrophoresis (PFGE) using a
398 CHEF-DRII system (Bio-Rad). The 200 kb DNA segment containing *TerB* sequences
399 within the gel was located by performing Southern hybridization on a portion of the gel
400 using a specific probe made from the pWB15 plasmid. This identified the pulse field gel
401 slice containing *TerB* sequences which was excised and melted (20 min at about 72°C).
402 The DNA in the gel solution was stretched on microscope slides coated with 3-
403 aminopropyltriethoxysilane, denatured with sodium hydroxide in ethanol, fixed with
404 glutaraldehyde and hybridized overnight with biotinylated DNA FISH probes at 37°C in
405 a humidified chamber. Biotinylated DNA FISH probes were made from the fosmid WI2-
406 1478M20 and from the plasmid pWB15. Following hybridization, slides were blocked
407 with 3% BSA for at least 20 min and incubated with the avidin Alexa Fluor 350. This was
408 followed by two rounds of incubation with the biotinylated anti-avidin D for 20 min
409 followed by the avidin Alexa Fluor 350 for 20 min. Slides were then incubated with an
410 antibody specific for IdU; a mouse anti-BrdU antibody, an antibody specific for CldU; a
411 rat monoclonal anti-BrdU antibody, and the biotinylated anti-avidin D for one hr. This
412 was followed by incubation with secondary antibodies: Alexa Fluor 568 goat anti-mouse
413 IgG (H+L), Alexa Fluor 488 goat anti-rat IgG (H+L), and the avidin Alexa Fluor 350 for
414 one hour. Slides were rinsed in PBS with 0.03% IGEPAL CA-630 after each incubation.
415 After the last rinse in PBS/CA-630, coverslips were mounted on the slides with Prolong
416 gold antifade reagent. A Zeiss fluorescent microscope and IP Lab software
417 (Scanalytics) were used to capture images of IdU/CldU incorporated DNA molecules.
418 Images were processed using Adobe Photoshop and aligned (using Adobe Illustrator)
419 based on the positions of FISH signals that identify the 200 kb segments that contain
420 the ter sequences.

421 **Proximity Ligation Assay (PLA)**

422 MCF7 5C-TerB cells were seeded on poly-L-lysine coated coverslips and transfected
423 the day after as described before. 24h hours after transfection, cells were washed with

424 PBS, and fixed and permeabilized with 4% paraformaldehyde containing 0.2% Triton X-
425 100 for 20min on ice and blocked with PBS-BSA 3% overnight at 4. Coverslips were
426 incubated with primary antibodies (see Table 1 for dilution) for 1h at RT. Proximity
427 ligation was performed using the Duolink® In Situ Red Starter Kit Mouse/Rabbit (Sigma-
428 Aldrich) according to the manufacturer's protocol. The oligonucleotides and antibody-
429 nucleic acid conjugates used were those provided in the Sigma-Aldrich PLA kit. Images
430 were quantified by counting the number of foci per nucleus using Nikon software.

431 **Immunoprecipitation**

432 For immunoprecipitation, MCF7 5C-TerB cells were pre-extracted using CSK100 buffer
433 (100 mM NaCl, 300mM sucrose, 3 mM MgCl2, 10 mM PIPES pH 6.8, 1 mM EGTA,
434 0.2% Triton X-100, anti-protease and anti-phosphatase) for 5 min on ice, fixed in 1%
435 formaldehyde for 10 min on ice and a 1% glycine solution was used to stop the reaction.
436 After scraping the cells in ice-cold PBS and centrifugation, pellets were lysed in SDS
437 lysis buffer (50 mM Tris-HCl pH 7.5, 150 mM NaCl, 0.1% SDS, anti-proteases and anti-
438 phosphatases) for 10 min on ice and sheared for 3 min. Samples were cleared by
439 centrifugation for 5 min at 4°C. Immunoprecipitations were performed on 10-fold diluted
440 lysates in dilution buffer (50 mM Tris-HCl pH 7.5, 150 mM NaCl,5 mM EDTA, 0.2%
441 Triton X-100, anti-proteases and anti-phosphatases). with antibodies against GFP,
442 γH2AX or IgG overnight at 4°C on a wheel. Beads were extensively washed in the
443 dilution buffer and denatured in 2X Laemmli buffer.

444 Proteins were separated on 4-12% acrylamide SDS-PAGE, transferred on
445 Nitrocellulose membrane and detected with the indicated antibodies described in the
446 table and ECL reagents.

447 **Cellular fractionation**

448 For the cellular fractionation, MCF7 5C-TerB cells were scraped in PBS, divided in 2
449 different tubes (1/3 of the volume for the whole cell extract (WCE) and the remaining 2/3
450 for the fractionation) and centrifuged to keep the pellets.

451 For the WCE, cells were lysed in 1 volume of lysis buffer (50 mM Tris Ph 7.5, 20 Mm
452 NaCl, 1 Mm MgCl2, 0.1% SDS, anti-protease and anti-phosphatase) for 10 min at RT
453 on a wheel and denaturated in 2X Laemmli buffer.

454 For the fractionation, MCF7 5C-TerB cells were pre-extracted in 2 volumes of CSK100
455 (100 mM NaCl, 300mM sucrose, 3 mM MgCl2, 10 mM pipes pH 6.8, 1 mM EGTA, 0.2%
456 Triton X-100, anti-protease and anti-phosphatase) for 15 min on ice, and centrifuged.
457 The supernatant (SN) representing the soluble fraction was kept in a new tube (soluble
458 fraction). The pellet was washed with CSK50 (50 mM NaCl, 300mM sucrose, 3 mM
459 MgCl2, 10 mM pipes pH 6.8, 1 mM EGTA, 0.2% Triton X-100, anti-protease and anti-
460 phosphatase and resuspended in 2 volumes of CSK50 containing benzonase for 10 min
461 on a rotating wheel, and the SN was kept after centrifugation (chromatin fraction). All
462 the fractions were denaturated in 2X Laemmli buffer.

463 Proteins were separated on 4-12% acrylamide SDS-PAGE, transferred on
464 Nitrocellulose membrane and detected with the indicated antibodies described in the
465 table and ECL reagents.

466 **Chromatin Immunoprecipitation Assay**

467 ChIPs were performed using the ChIP-IT express according to manufacturer's
468 instructions. Cells were crosslinked, washed, harvested by scraping and lysed
469 according to the kit instructions. Chromatin was sonicated to 200-1500 bp fragments
470 and DNA concentration determined. Equal amount up to 15 ug of DNA was then used
471 for each immunoprecipitation. Antibodies used were listed on the table below. DNA
472 fragments were eluted, purified, and analyzed by SYBR Green real-time PCR.
473 Sequences of primers used for qPCR are given in the table. Experiments were
474 repeated at least three times and each real time qPCR reaction was performed in
475 duplicate.

476 **Detection of DSBs using the T7 endonuclease assay**

477 MCF7 5C-TerB cells were seeded and transfected the day after with 120 pmol of Cas9
478 protein and 120 pmol of the sgRNA TerB1 using the Lipofectamine CRISPRMAX™
479 Cas9 transfection reagents (previously described). 24 hours post-transfection, cells

480 were lysed using a lysis buffer (100 mM NaCl, 10 mM Tris-HCl pH 8, 25 mM EDTA pH
481 8, 0,5% SDS) and 50 ug of Proteinase K overnight at 50°C with shaking. After addition
482 of NaCl and mix for 1 min, the supernatant was put in a new tube and an ethanol
483 precipitation was performed. A PCR to amplify the 900 bp region surrounding the
484 sgRNA TerB1 site was conducted using PP9F and R. Heteroduplex were formed by
485 heating and cooling down the samples and a T7 endonuclease assay digestion was
486 performed prior electrophoresis for detection.

487 **Cell Cycle progression**

488 MCF7 5C-TerB cells were transfected as described before. Control cells were treated
489 with 2mM HU for 4 hours before harvesting. Cells were washed with PBS and fixed in 1
490 ml cold 70% ethanol for 30 minutes. Cells were pelleted and washed with PBS. 100
491 µg/mL RNase A was added 50 µg/mL PI solution was added directly to the pellet, mixed
492 well and incubated for 30 mins at room temperature in the dark. 50,000 cells per
493 condition were analyzed by flow cytometry.

494 **Immunofluorescence (γH2AX)**

495 Cells were fixed with 4% PFA/PBS for 20 min, permeabilized with 0.5% Triton-X 100 for
496 10 min, washed 3 times in 1X PBS, and blocked in 10% goat serum overnight at 4°C.
497 The primary antibody (1:500) was incubated for 2 hr at room temperature. Cells were
498 then washed 3 times in 1X PBS. The secondary antibody (1:1500) was incubated for 1
499 hr at room temperature in dark. Cells were then washed again 3 times in 1X PBS.
500 Stained cells were mounted with mounting medium containing DAPI. Slides were
501 imaged at 60X (immersion oil) using Nikon A1 spinning disk confocal microscope.

502 **Image Analysis**

503 For PLA and gH2AX experiments, slides were imaged at 60X (immersion oil) with Nikon
504 spinning disk confocal microscope. PLA foci per nucleus and gH2AX foci per nucleus
505 were calculated using Nikon Elements AR Analysis Explorer (version 5.21.03), where
506 DAPI was used as a mask for the nucleus. The number of PLA foci per nucleus were
507 quantified to get the percentage of cells with 1 or 2 foci indicating a positive signal at the

site-specific replication block. The number of gH2AX foci was counted for each DAPI to obtain the average number of gH2AX foci in each condition.

NGS sequencing of the MCF7 5C-TerB clone

Genomic DNA was extracted from the cells and submitted to Novogene for sequencing. The samples were processed and whole genome sequencing was performed using their hWGS service pipeline.

Data analysis and Statistics

Statistical analysis for the various experiments was performed using GraphPad Prism version 9.4.0. Results are presented as mean ± standard error of the mean (SEM). A p value of <0.05 by Student's t-test was considered statistically significant. ns: non-significant, * Indicates p<0.05, **: P<0.005, ***: P<0.001.

Data availability

The list of antibodies, plasmids and oligonucleotides used in this study are provided in Supplementary Table 2. WGS sequencing files generated in this study have been deposited at the Gene Expression Omnibus (GEO) database under accession number PRJNA868342 and are publicly available as of the date of publication. Any additional information required to reanalyze the data reported in this paper is available from the lead contact upon request.

Acknowledgments

We are indebted to Ino de Bruijn, Jorge S. Reis-Filho, and Yingjie Zhu for help with the genomics data. We thank members of the Powell and Schildkraut lab for their comments on the manuscript. This work was supported in part by NIH Grants R01-CA187069 and P50-CA247749 (to S.N.P.); 5R01-GM045751 and R01-CA085344 (to C.L.S.); National Cancer Institute Cancer Center Support Grants, P30-CA008748 at MSK, and P30-CA013330 for use of a core facility at Albert Einstein COM. S.T. was

supported by NIH Training Grant T-32 NIH 5T32AG023475. Figures were created with the aid of BioRender.

Author Contributions

Conceptualization, S.N.P., S.A.S. and C.L.S.; Methodology, S.N.P., S.A.S., M.J., H.E.G., A.S., C.T. and C.L.S; Validation, S.A.S, M.J. and C.L.S.; Formal Analysis, S.A.S, M.J., H.E.G., A.S., C.T. and C.L.S.; Investigation, S.A.S, M.J., S.T., H.E.G., A.S., C.T. and S.T.K. ; Resources, S.N.P. and C.L.S ; Writing – Original Draft, S.A.S., M.J., H.E.G., A.S. and S.N.P.; Writing – Review & Editing, C.L.S and S.T.K.; Visualization, S.A.S., M.J., H.E.G. and A.S.; Supervision, S.N.P. and C.L.S.; Project Administration, S.N.P. and C.L.S.; Funding Acquisition, S.N.P. and C.L.S.

Competing interests

The authors declare no competing interests.

References

Bakkenist CJ, Kastan MB. 2003. DNA damage activates ATM through intermolecular autophosphorylation and dimer dissociation. *Nature 2003 421:6922* **421**:499–506. doi:10.1038/nature01368

Bantele SCS, Lisby M, Pfander B. 2019. Quantitative sensing and signalling of single-stranded DNA during the DNA damage response. *Nature Communications 2019 10:1* **10**:1–12. doi:10.1038/s41467-019-08889-5

Berkovich E, Monnat RJ, Kastan MB. 2007. Roles of ATM and NBS1 in chromatin structure modulation and DNA double-strand break repair. *Nat Cell Biol* **9**:683–690. doi:10.1038/NCB1599

Brickner JR, Garzon JL, Cimprich KA. 2022. Walking a tightrope: The complex balancing act of R-loops in genome stability. *Mol Cell* **82**. doi:10.1016/J.MOLCEL.2022.04.014

Bryan TM. 2019. Mechanisms of DNA Replication and Repair: Insights from the Study of G-Quadruplexes. *Molecules 2019, Vol 24, Page 3439* **24**:3439. doi:10.3390/MOLECULES24193439

Chailleux C, Aymard F, Caron P, Daburon V, Courilleau C, Canitrot Y, Legube G, Trouche D. 2014. Quantifying DNA double-strand breaks induced by site-specific endonucleases in living cells by ligation-mediated purification. *Nat Protoc* **9**:517–528. doi:10.1038/NPROT.2014.031

Chandramouly G, Kwok A, Huang B, Willis NA, Xie A, Scully R. 2013. BRCA1 and CtIP suppress long-tract gene conversion between sister chromatids. *Nat Commun* **4**. doi:10.1038/NCOMMS3404

Clouaire T, Rocher V, Lashgari A, Arnould C, Aguirrebengoa M, Biernacka A, Skrzypczak M, Aymard F, Fongang B, Dojer N, Iacovoni JS, Rowicka M, Ginalski K, Côté J, Legube G. 2018. Comprehensive Mapping of Histone Modifications at DNA Double-Strand Breaks Deciphers Repair Pathway Chromatin Signatures. *Mol Cell* **72**:250-262.e6. doi:10.1016/J.MOLCEL.2018.08.020

Collis SJ, Ciccia A, Deans AJ, Hořejší Z, Martin JS, Maslen SL, Skehel JM, Elledge SJ, West SC, Boulton SJ. 2008. FANCM and FAAP24 function in ATR-mediated checkpoint signaling independently of the Fanconi anemia core complex. *Mol Cell* **32**:313–324. doi:10.1016/J.MOLCEL.2008.10.014

Dixon JR, Selvaraj S, Yue F, Kim A, Li Y, Shen Y, Hu M, Liu JS, Ren B. 2012. Topological domains in mammalian genomes identified by analysis of chromatin interactions. *Nature* **485**:376–380. doi:10.1038/NATURE11082

Drosopoulos WC, Kosiyatrakul ST, Yan Z, Calderano SG, Schildkraut CL. 2012. Human telomeres replicate using chromosome-specific, rather than universal, replication programs. *Journal of Cell Biology* **197**:253–266. doi:10.1083/JCB.201112083

Drosopoulos WC, Vierra DA, Kenworthy CA, Coleman RA, Schildkraut CL. 2020. Dynamic Assembly and Disassembly of the Human DNA Polymerase δ Holoenzyme on the Genome In Vivo. doi:10.1016/j.celrep.2019.12.101

Elango R, Panday A, Lach FP, Willis NA, Nicholson K, Duffey EE, Smogorzewska A, Scully R. 2022. The structure-specific endonuclease complex SLX4-XPF regulates Tus-Ter-induced homologous recombination. *Nat Struct Mol Biol* **29**:801–812. doi:10.1038/S41594-022-00812-9

Fokas E, Prevo R, Pollard JR, Reaper PM, Charlton PA, Cornelissen B, Vallis KA, Hammond EM, Olcina MM, Gillies McKenna W, Musche RJ, Brunner TB. 2012. Targeting ATR in vivo using the novel inhibitor VE-822 results in selective sensitization of pancreatic tumors to radiation. *Cell Death & Disease 2012 3:12* **3**:e441–e441. doi:10.1038/cddis.2012.181

Gaillard H, García-Muse T, Aguilera A. 2015. Replication stress and cancer. *Nat Rev Cancer* **15**:276–280. doi:10.1038/NRC3916

Helt CE, Wang W, Keng PC, Bambara RA. 2005. 9-1-1 Complex Involvement in DNA Repair: Evidence that DNA Damage Detection Machinery Participates in DNA Repair. *http://dx.doi.org/104161/cc441598* **4**:529–532. doi:10.4161/CC.4.4.1598

Hiasa H, Marians KJ. 1994. Tus prevents overreplication of oriC plasmid DNA. *Journal of Biological Chemistry* **269**:26959–26968. doi:10.1016/S0021-9258(18)47112-8

Hidaka M, Akiyama M, Horiuchi T. 1988. A consensus sequence of three DNA replication terminus sites on the E. coli chromosome is highly homologous to the terR sites of the R6K plasmid. *Cell* **55**:467–475. doi:10.1016/0092-8674(88)90033-5

Iyer DR, Rhind N. 2017. The Intra-S Checkpoint Responses to DNA Damage. *Genes (Basel)* **8**. doi:10.3390/GENES8020074

Iyer DR, Rhind N. 2013. Checkpoint regulation of replication forks: global or local? *Biochem Soc Trans* **41**:1701–1705. doi:10.1042/BST20130197

Kaufmann WK, Cleaver JE, Painter RB. 1980. Ultraviolet radiation inhibits replicon initiation in S phase human cells. *Biochim Biophys Acta* **608**:191–195. doi:10.1016/0005-2787(80)90147-1

Kim JC, Harris ST, Dinter T, Shah KA, Mirkin SM. 2016. The role of break-induced replication in large-scale expansions of (CAG)n/(CTG)n repeats. *Nature Structural & Molecular Biology 2016 24:1* **24**:55–60. doi:10.1038/nsmb.3334

Larsen NB, Hickson ID, Mankouri HW. 2014a. Tus-Ter as a tool to study site-specific DNA replication perturbation in eukaryotes. *Cell Cycle* **13**:2994. doi:10.4161/15384101.2014.958912

Larsen NB, Sass E, Suski C, Mankouri HW, Hickson ID. 2014b. The Escherichia coli Tus–Ter replication fork barrier causes site-specific DNA replication perturbation in yeast. *Nature Communications 2014 5:1* **5**:1–10. doi:10.1038/ncomms4574

Marie L, Symington LS. 2022. Mechanism for inverted-repeat recombination induced by a replication fork barrier. *Nature Communications 2022 13:1* **13**:1–13. doi:10.1038/s41467-021-27443-w

Merrick CJ, Jackson D, Diffley JFX. 2004. Visualization of altered replication dynamics after DNA damage in human cells. *J Biol Chem* **279**:20067–20075. doi:10.1074/JBC.M400022200

632 Mirkin E v., Mirkin SM. 2007. Replication Fork Stalling at Natural Impediments. *Microbiol*
633 *Mol Biol Rev* **71**:13. doi:10.1128/MMBR.00030-06

634 Mulcair MD, Schaeffer PM, Oakley AJ, Cross HF, Neylon C, Hill TM, Dixon NE. 2006. A
635 molecular mousetrap determines polarity of termination of DNA replication in E.
636 coli. *Cell* **125**:1309–1319. doi:10.1016/J.CELL.2006.04.040

637 Nandi S, Whitby MC. 2012. The ATPase activity of Fml1 is essential for its roles in
638 homologous recombination and DNA repair. *Nucleic Acids Res* **40**:9584–9595.
639 doi:10.1093/NAR/GKS715

640 Norio P, Schildkraut CL. 2001. Visualization of DNA replication on individual Epstein-
641 Barr virus episomes. *Science* **294**:2361–2364. doi:10.1126/SCIENCE.1064603

642 Panday A, Willis NA, Elango R, Menghi F, Duffey EE, Liu ET, Scully R. 2021. FANCM
643 regulates repair pathway choice at stalled replication forks. *Mol Cell* **81**:2428-
644 2444.e6. doi:10.1016/J.MOLCEL.2021.03.044/ATTACHMENT/DB09DDDE-5057-
645 4829-A9A6-753D68F31F16/MMC1.PDF

646 Parrilla-Castellar ER, Arlander SJH, Karnitz L. 2004. Dial 9–1–1 for DNA damage: the
647 Rad9–Hus1–Rad1 (9–1–1) clamp complex. *DNA Repair (Amst)* **3**:1009–1014.
648 doi:10.1016/J.DNAREP.2004.03.032

649 Rao SSP, Huntley MH, Durand NC, Stamenova EK, Bochkov ID, Robinson JT, Sanborn
650 AL, Machol I, Omer AD, Lander ES, Aiden EL. 2014. A 3D map of the human
651 genome at kilobase resolution reveals principles of chromatin looping. *Cell*
652 **159**:1665–1680. doi:10.1016/J.CELL.2014.11.021

653 Roecklein B, Pelletier A, Kuempel P. 1991. The tus gene of Escherichia coli:
654 autoregulation, analysis of flanking sequences and identification of a
655 complementary system in Salmonella typhimurium. *Res Microbiol* **142**:169–175.
656 doi:10.1016/0923-2508(91)90026-7

657 Savic V, Yin B, Maas NL, Bredemeyer AL, Carpenter AC, Helmink BA, Yang-Iott KS,
658 Sleckman BP, Bassing CH. 2009. Formation of dynamic gamma-H2AX domains
659 along broken DNA strands is distinctly regulated by ATM and MDC1 and

660 dependent upon H2AX densities in chromatin. *Mol Cell* **34**:298–310.
661 doi:10.1016/J.MOLCEL.2009.04.012

662 Saxena S, Zou L. 2022. Hallmarks of DNA replication stress. *Mol Cell* **82**:2298–2314.
663 doi:10.1016/J.MOLCEL.2022.05.004

664 Shimada K, Pasero P, Gasser SM. 2002. ORC and the intra-S-phase checkpoint: a
665 threshold regulates Rad53p activation in S phase. *Genes Dev* **16**:3236–3252.
666 doi:10.1101/GAD.239802

667 Tubbs A, Nussenzweig A. 2017. Endogenous DNA Damage as a Source of Genomic
668 Instability in Cancer. *Cell* **168**:644–656. doi:10.1016/J.CELL.2017.01.002

669 Twayana S, Bacolla A, Barreto-Galvez A, De-Paula RB, Drosopoulos WC, Kosiyatrakul
670 ST, Bouhassira EE, Tainer JA, Madireddy A, Schildkraut CL. 2021. Translesion
671 polymerase eta both facilitates DNA replication and promotes increased human
672 genetic variation at common fragile sites. *Proc Natl Acad Sci U S A*
673 **118**:e2106477118.
674 doi:10.1073/PNAS.2106477118/SUPPL_FILE/PNAS.2106477118.SD03.XLSX

675 Ward IM, Chen J. 2001. Histone H2AX Is Phosphorylated in an ATR-dependent Manner
676 in Response to Replicational Stress. *Journal of Biological Chemistry* **276**:47759–
677 47762. doi:10.1074/jbc.C100569200

678 Willis N, Rhind N. 2009a. Regulation of DNA replication by the S-phase DNA damage
679 checkpoint. *Cell Div* **4**:1–10. doi:10.1186/1747-1028-4-13/COMMENTS

680 Willis N, Rhind N. 2009b. Regulation of DNA replication by the S-phase DNA damage
681 checkpoint. *Cell Div* **4**. doi:10.1186/1747-1028-4-13

682 Willis NA, Chandramouly G, Huang B, Kwok A, Follonier C, Deng C, Scully R. 2014.
683 BRCA1 controls homologous recombination at Tus/Ter-stalled mammalian
684 replication forks. *Nature* **510**:556–559. doi:10.1038/NATURE13295

685 Willis NA, Frock RL, Menghi F, Duffey EE, Panday A, Camacho V, Hasty EP, Liu ET, Alt
686 FW, Scully R. 2017. Mechanism of tandem duplication formation in BRCA1-mutant
687 cells. *Nature 2017 551:7682* **551**:590–595. doi:10.1038/nature24477

Willis NA, Panday A, Duffey EE, Scully R. 2018. Rad51 recruitment and exclusion of non-homologous end joining during homologous recombination at a Tus/Ter mammalian replication fork barrier. *PLoS Genet* **14**. doi:10.1371/JOURNAL.PGEN.1007486

Willis NA, Scully R. 2016. Spatial separation of replisome arrest sites influences homologous recombination quality at a Tus/Ter-mediated replication fork barrier. *Cell Cycle* **15**:1812–1820. doi:10.1080/15384101.2016.1172149

Xue X, Sung P, Zhao X. 2015. Functions and regulation of the multitasking FANCM family of DNA motor proteins. *Genes Dev* **29**:1777–1788. doi:10.1101/GAD.266593.115

Zeman MK, Cimprich KA. 2013. Causes and consequences of replication stress. *Nature Cell Biology 2014 16:1* **16**:2–9. doi:10.1038/ncb2897

Figures

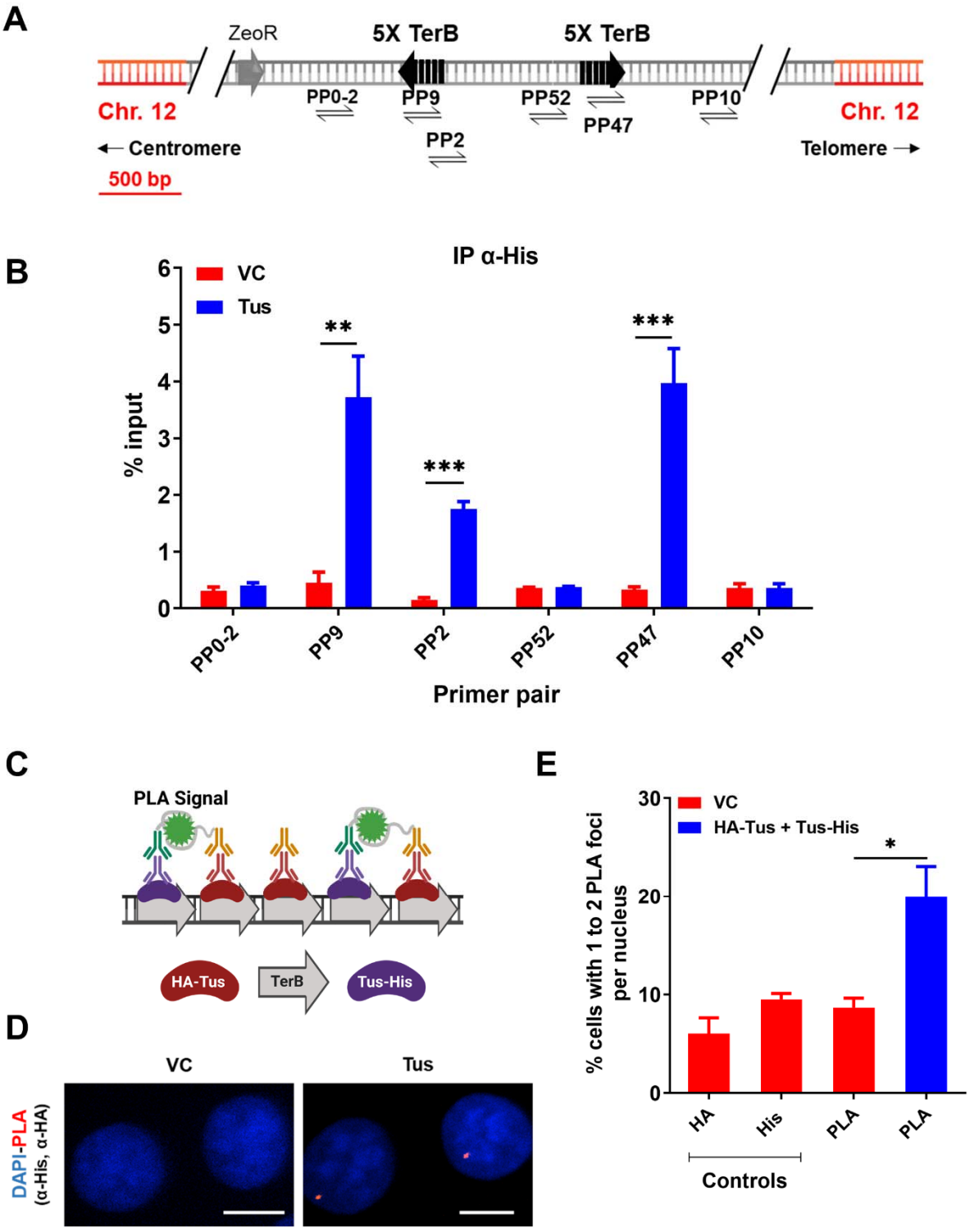
A
ZeoR
5X TerB
5X TerB
Chr. 12
PP0-2
PP9
PP52
PP10
Chr. 12
PP47
PP2
Centromere
Telomere
500 bp
B
IP α-His
VC
Tus
% input
**
***
***
PP0-2
PP9
PP2
PP52
PP47
PP10
Primer pair
C
PLA Signal
HA-Tus
TerB
Tus-His
D
VC
Tus
DAPI-PLA
(α-His, α-HA)
E
VC
HA-Tus + Tus-His
*
% cells with 1 to 2 PLA foci per nucleus
HA
His
PLA
PLA
Controls

703 **Figure 1:**

704 **Figure 1. Tus is bound to *TerB* sites integrated in human cells: (A)** Schematic of
705 linearized plasmid (pWB15) integrated into MCF7 cells (MCF7 5C-TerB) with two
706 cassettes containing 5 tandem *TerB* sequences in the non-permissive orientation (black
707 arrows). Black half-arrow heads depict PCR products expected from stated primer pairs
708 used in. **(B)** ChIP with His antibody on MCF7 5C-TerB cells transfected with either a
709 vector control (VC) or HA-Tus-His expression plasmids. ChIP-qPCR were conducted
710 using the indicated primer pairs. Data show the percentage of input (n=3). **(C)**
711 Schematic of PLA to visualize Tus bound to *TerB* sites using HA and His antibodies. **(D)**
712 Representative images of the PLA foci across stated conditions. Bars, 10 µm **(E)**
713 Percentage of cells with 1-2 PLA foci per nucleus. (n=3, ≥150 cells per experiment).

714

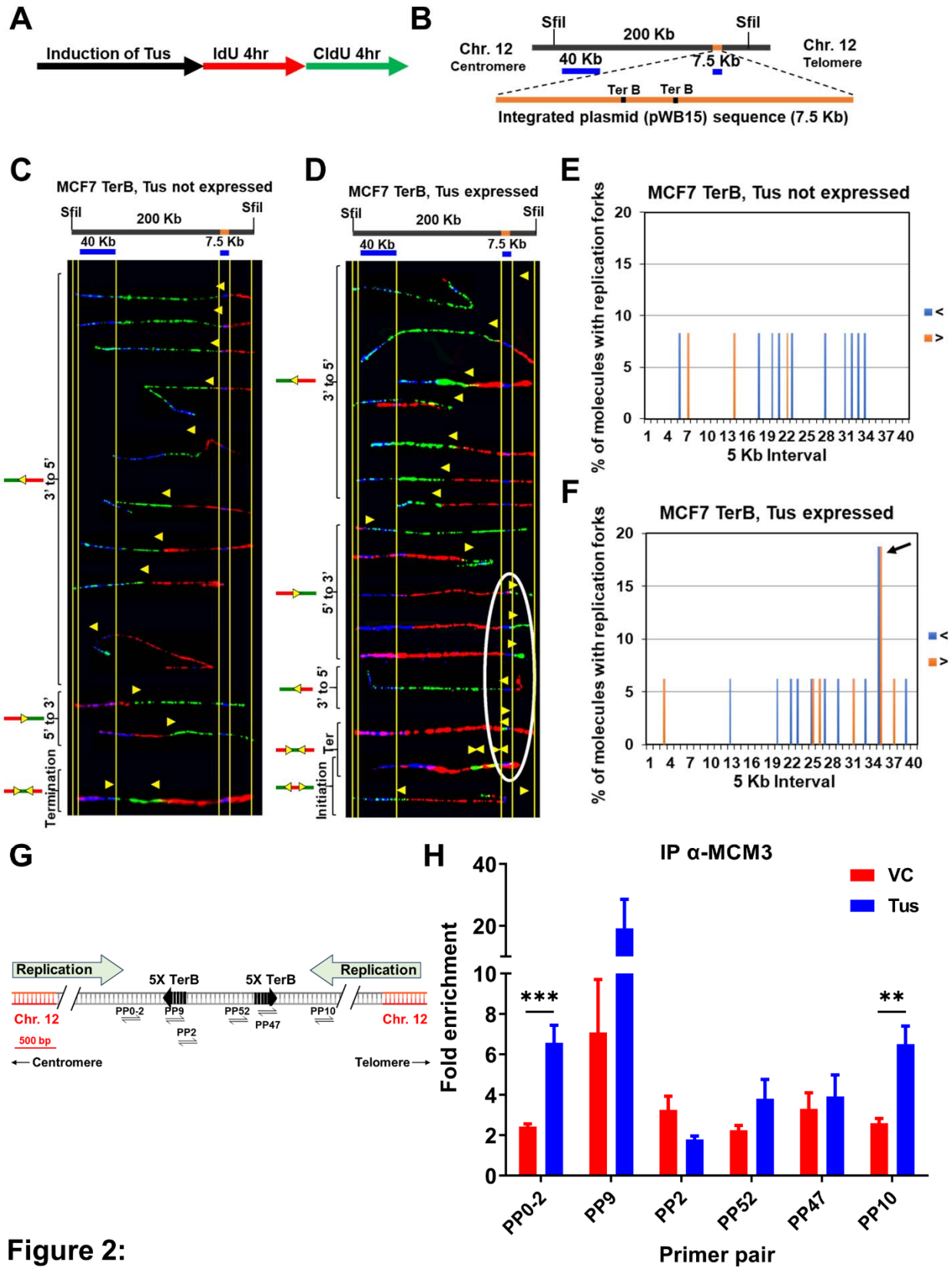
A
Induction of Tus
IdU 4hr
CldU 4hr
B
SfiI
200 Kb
SfiI
Chr. 12
Centromere
40 Kb
7.5 Kb
Chr. 12
Telomere
Ter B
Ter B
Integrated plasmid (pWB15) sequence (7.5 Kb)
C
MCF7 TerB, Tus not expressed
SfiI
200 Kb
SfiI
40 Kb
7.5 Kb
3' to 5'
5' to 3'
Termination
D
MCF7 TerB, Tus expressed
SfiI
200 Kb
SfiI
40 Kb
7.5 Kb
3' to 5'
5' to 3'
3' to 5'
Ter
Initiation
E
MCF7 TerB, Tus not expressed
% of molecules with replication forks
5 Kb Interval
F
MCF7 TerB, Tus expressed
% of molecules with replication forks
5 Kb Interval
G
Replication
5X TerB
5X TerB
Replication
Chr. 12
PP0-2
PP9
PP52
PP10
Chr. 12
PP2
PP47
500 bp
Centromere
Telomere
H
IP α-MCM3
VC
Tus
Fold enrichment
***
**
PP0-2
PP9
PP2
PP52
PP47
PP10
Primer pair

Figure 2:

716 **Figure 2. Replication fork pauses at the Ter sequence in the presence of the Tus**
717 **protein: (A)** Schematic of pulse labelling of MCF7 5C-TerB cells with Tus protein
718 expression for 3 days. **(B)** Locus map of a 200 kb SfiI segment from MCF7 5C-TerB
719 Chromosome 12 with the integrated plasmid (pWB15) DNA (orange). A 40 kb FISH
720 probe made from fosmid WI2-1478M20 and a 7.5 kb FISH probe made from plasmid
721 pWB15 are shown in blue. **(C-D)** Top: locus map of the DNA segment containing *Ter*
722 sequence with the location of the FISH probes. Bottom: photomicrographs of labeled
723 DNA molecules from MCF7 5C-TerB, Tus not expressed **(C)** and MCF7 5C-TerB, Tus
724 expressed **(D)**. Yellow arrows indicate the position of replication forks at the transition of
725 labeling from IdU to CldU incorporation showing replication fork direction. Molecules are
726 arranged in the following order: forks progressing from 3' to 5', forks progressing from 5'
727 to 3', termination events, and initiation events. Replication forks (Yellow Arrows) in the
728 white oval are all at the same location (at the *TerB* sequence) on molecules from
729 different cells indicating that replication forks are pausing at this *TerB* sequence. **(E-F)**
730 Percentage of molecules with replication forks at each 5 Kb interval in the 200 Kb SfiI
731 segment containing *TerB* sequence, quantified from molecules in MCF7 5C-TerB **(E)**
732 Tus not expressed and (**F)** Tus expressed. Percentage of molecules with replication
733 forks progressing 3' to 5' (< blue) and 5' to 3' (> orange) are shown. In the cells
734 expressing Tus, a high percentage of molecules contain replication forks pausing in
735 both directions in the 5 Kb interval which contains Ter sequences (black arrow **(F)**, white
736 oval **(D)**). **(G)** Schematic similar to Fig1A with progression of the endogenous origins of
737 replication within the chromosome 12 shown (green arrows). **(H)** ChIP using MCM3
738 antibody on MCF7 5C-TerB cells transfected with VC or HA-Tus-His plasmids. ChIP-
739 qPCR were conducted using the indicated primer pairs. Data shows the fold enrichment
740 relative to the IgG controls (n=3).

741

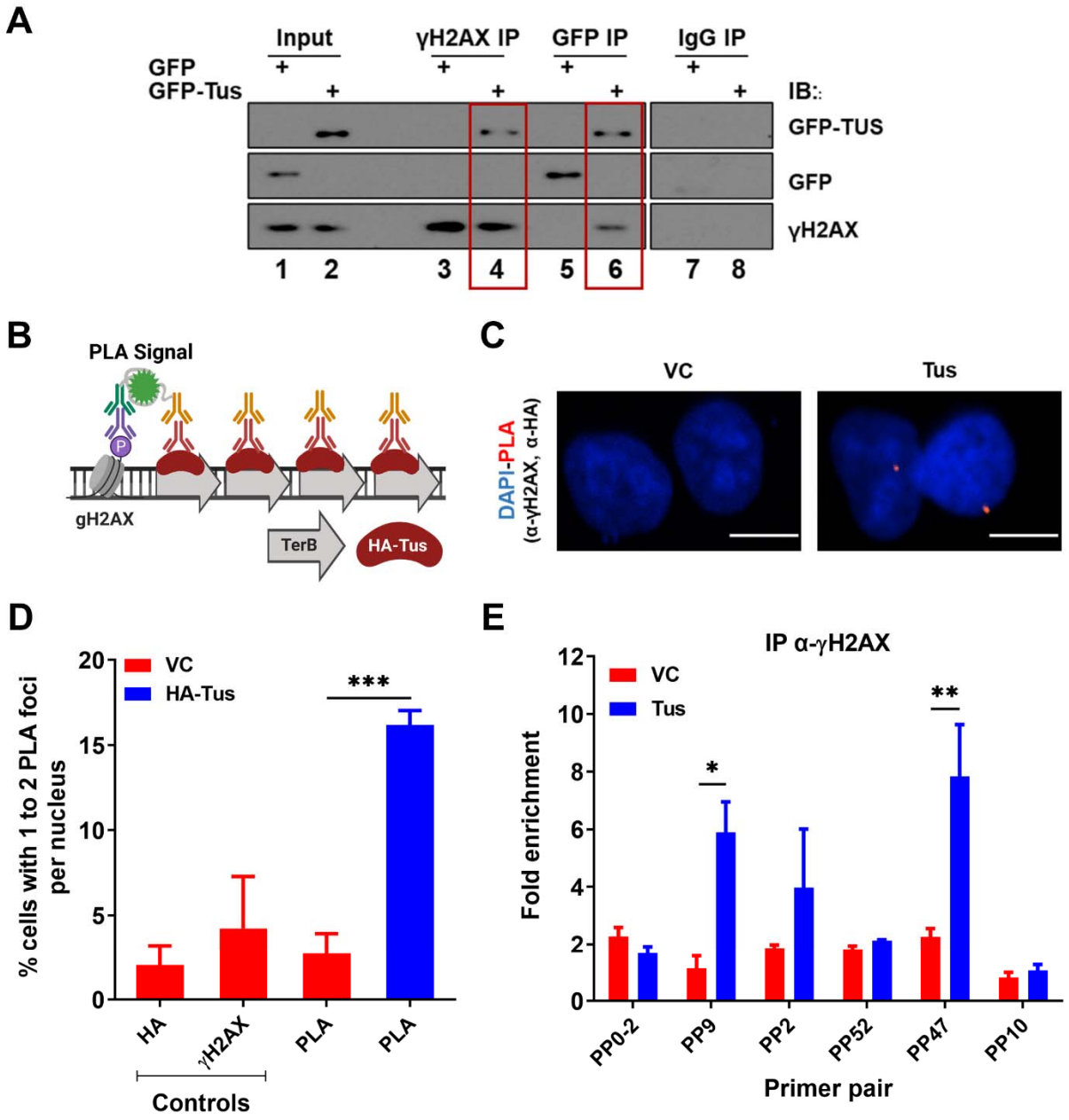
A
Input
γH2AX IP
GFP IP
IgG IP
GFP
GFP-Tus
IB:
GFP-TUS
GFP
γH2AX
1 2 3 4 5 6 7 8
B
PLA Signal
gH2AX
TerB
HA-Tus
C
VC
Tus
DAPI-PLA
(α-γH2AX, α-HA)
D
VC
HA-Tus
% cells with 1 to 2 PLA foci per nucleus
***
HA
γH2AX
PLA
PLA
Controls
E
IP α-γH2AX
VC
Tus
Fold enrichment
*
**
PP0-2
PP9
PP2
PP52
PP47
PP10
Primer pair

742 **Figure 3:**

743 **Figure 3. γH2AX is enriched at *TerB* sites after Tus expression: (A)** MCF7 5C-TerB
744 cells transfected with GFP or GFP-Tus, γH2AX and IgG antibodies were used to
745 immuno-precipitate proteins and analysed by immunoblotting with indicated antibodies.
746 **(B)** Schematic of PLA to visualize HA-Tus bound to *TerB* in the proximity of γH2AX sites
747 using HA and γH2AX antibodies **(C)** Representative images of the PLA foci across
748 stated conditions. Bars, 10 μm **(D)** Percentage of cells with 1-2 PLA foci per nucleus.
749 (n=3, ≥150 cells per experiment). **(E)** γH2AX levels along the integrated *TerB* plasmid
750 were analyzed by ChIP-qPCR in MCF7 5C-TerB cells transfected with VC or Tus
751 expression plasmids using the indicated primer pairs. Data shows the fold enrichment
752 relative to IgG controls (n=3).

753

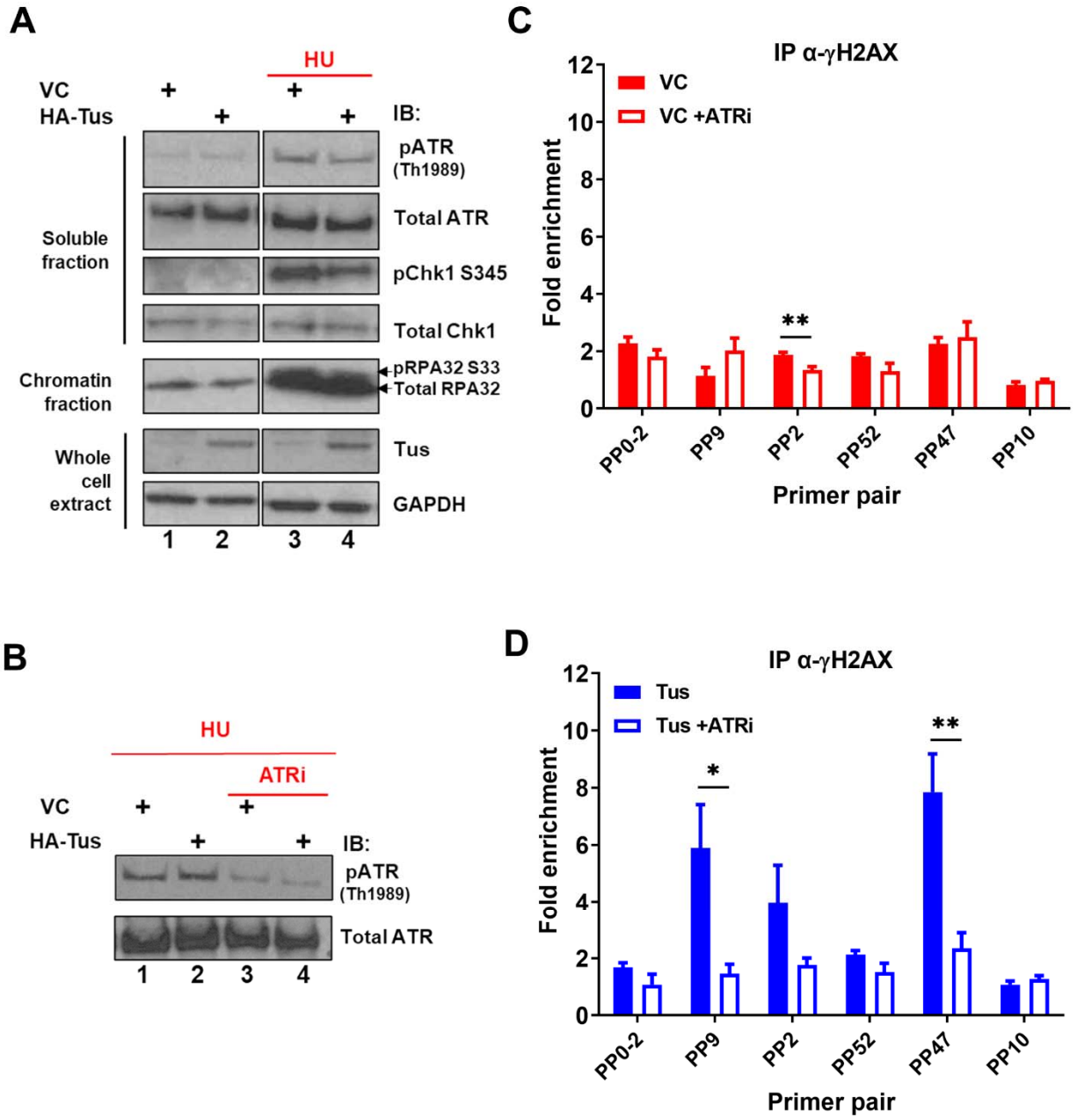
A
HU
VC
HA-Tus
IB:
pATR (Th1989)
Total ATR
Soluble fraction
pChk1 S345
Total Chk1
Chromatin fraction
pRPA32 S33
Total RPA32
Whole cell extract
Tus
GAPDH
1 2 3 4
B
HU
ATRi
VC
HA-Tus
IB:
pATR (Th1989)
Total ATR
1 2 3 4
C
IP α-γH2AX
VC
VC +ATRi
Fold enrichment
**
PP0-2
PP9
PP2
PP52
PP47
PP10
Primer pair
D
IP α-γH2AX
Tus
Tus +ATRi
Fold enrichment
*
**
PP0-2
PP9
PP2
PP52
PP47
PP10
Primer pair

754 **Figure 4:**

755 **Figure 4. γH2AX phosphorylation at Tus-*TerB* is ATR-dependent: (A)** MCF7 5C-
756 TerB cells transfected with VC or HA-Tus were treated for 4hrs with 2mM HU before
757 lysis and fractionation (whole cell extract (WCE), soluble fraction and chromatin
758 fraction). Total and phosphorylated protein levels were examined by immunoblotting as
759 indicated. Tus expression was confirmed in WCE. **(B)** Depletion of pATR Th1989 in
760 MCF7 5C-TerB cells treated with 2mM HU +/- 40 nM of ATR inhibitor was examined
761 with immunoblotting. **(C-D)** γH2AX levels were analyzed by ChIP-qPCR in MCF7 5C-
762 TerB cells transfected with **(C)** VC expression plasmid **(D)** Tus expression plasmid, +/-
763 4hrs treatment with ATRi with indicated primer pairs. Data shows the fold enrichment
764 over the IgG controls (n=3).

765

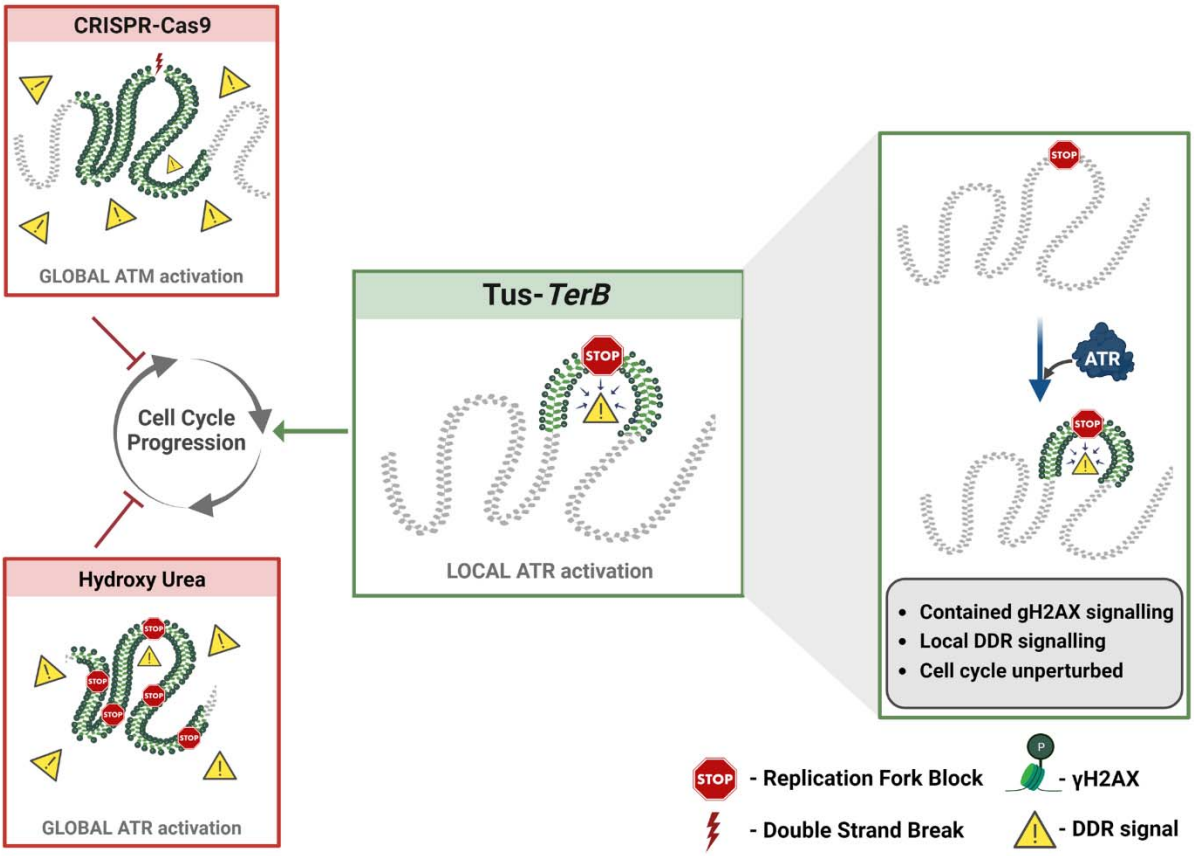
CRISPR-Cas9
GLOBAL ATM activation
Cell Cycle Progression
Hydroxy Urea
GLOBAL ATR activation
Tus-*TerB*
STOP
LOCAL ATR activation
ATR
• Contained gH2AX signalling
• Local DDR signalling
• Cell cycle unperturbed
- Replication Fork Block
- γH2AX
- Double Strand Break
- DDR signal

766 **Figure 5:**

767 **Figure 5. A local ATR-dependent checkpoint is activated by the Tus-*TerB* RFB.** A
768 model depicting the cellular response to a site-specific DSB using CRISPR-Cas9 and a
769 global replication stress with hydroxyurea, both of which lead to a DNA damage
770 response (DDR, yellow triangles), increased gH2AX (green) levels globally in the cell
771 and, if left unresolved, can alter cell cycle progression. In contrast, the site-specific
772 replication fork block, Tus/*TerB*, elicits a local ATR dependent DNA damage response
773 which is responsible for the phosphorylation and accumulation of γH2AX at the stalled
774 site. This local signaling does not affect the progression of the cell cycle is not altered
775 during the local checkpoint response.

776

Supplementary Figures

Sup Figure 1:

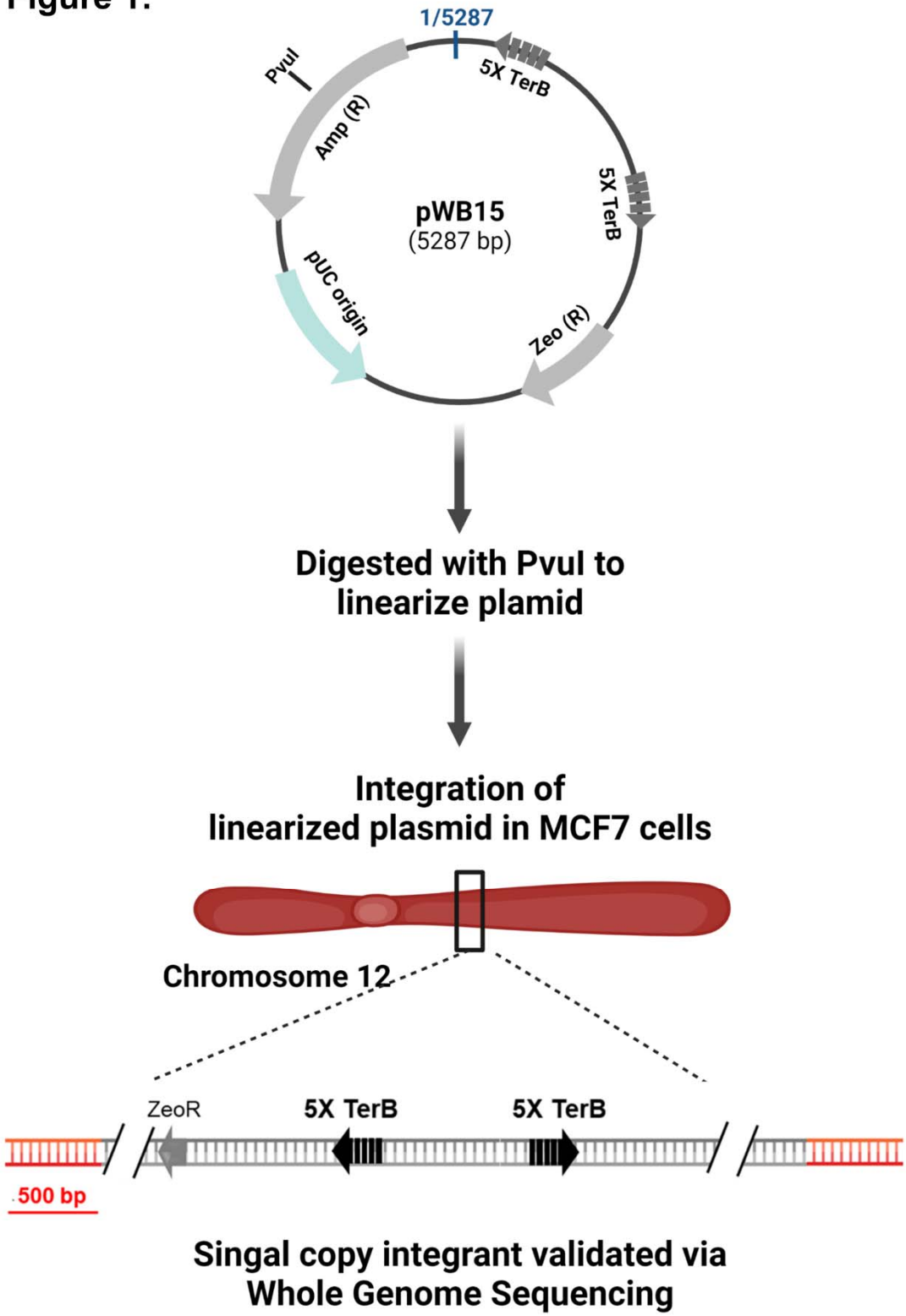

779 **Supplementary Figure 1. Generation of the MCF7 5C-TerB cell line:** Schematic of
780 the integration of pWB15 in MCF7 cells to generate MCF7 5C-TerB. pWB15 contains
781 two *TerB* cassettes (grey arrows). Each *TerB* cassette contains 5 tandem *TerB*
782 sequences, which are in the non-permissive orientation in pWB15 (grey arrow facing
783 away from each other. The plasmid was linearized by digesting with PvuI for integration
784 into MCF7 cells. The single copy integrant was confirmed using whole genome
785 sequencing and found to be integrated at Chromosome 12.

786

Sup Figure 2:

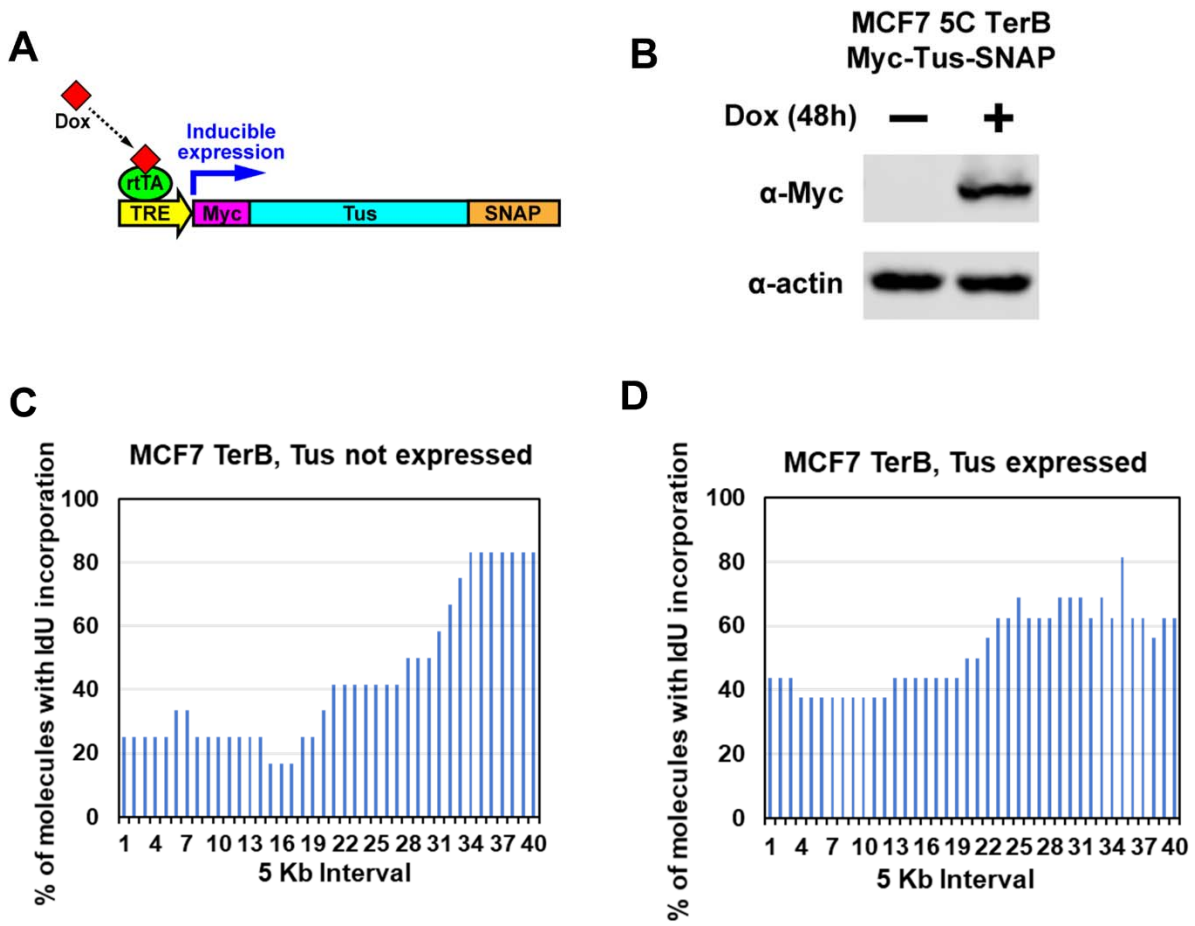

Supplementary Figure 2. **Expression of Tus in MCF7 5C-TerB cells: (A)** Schematic of Doxycycline (Dox) inducible expression of Myc-NLS-TUS-SNAP. (rtTA = reverse tetracycline trans activator; TRE = tetracycline response element). **(B)** Immunoblot of MCF7 5C-TerB cells stably expressing Dox inducible Myc-NLS-TUS-SNAP. **(C-D)** Replication profiles shown as the percentage of molecules with IdU incorporation at each 5 Kb interval in the 200 Kb SfiI segment containing *TerB* sequence, quantified from molecules MCF7 5C-TerB in Figure 2C (Tus not expressed) and Figure 2D (Tus expressed).

Sup Figure 3:

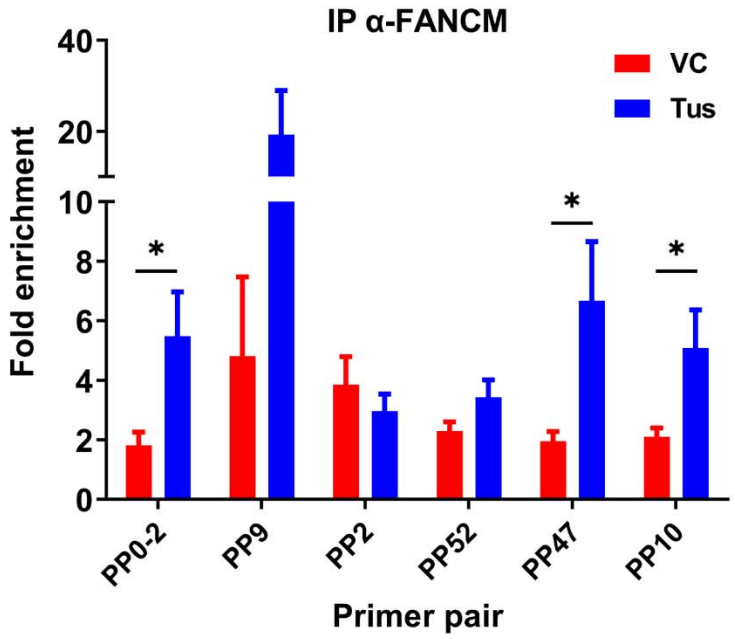

797

798 **Supplementary Figure 3. Enrichment of FANCM at the Ter sequence in the**
799 **presence of the Tus protein:** ChIP using FANCM antibody was performed MCF7 5C-
800 TerB cells transfected with VC or HA-Tus-His plasmids. ChIP-qPCR were conducted
801 using the indicated primer pairs. Data shows the fold enrichment relative to the IgG
802 controls (n=3).

803

Sup Figure 4.

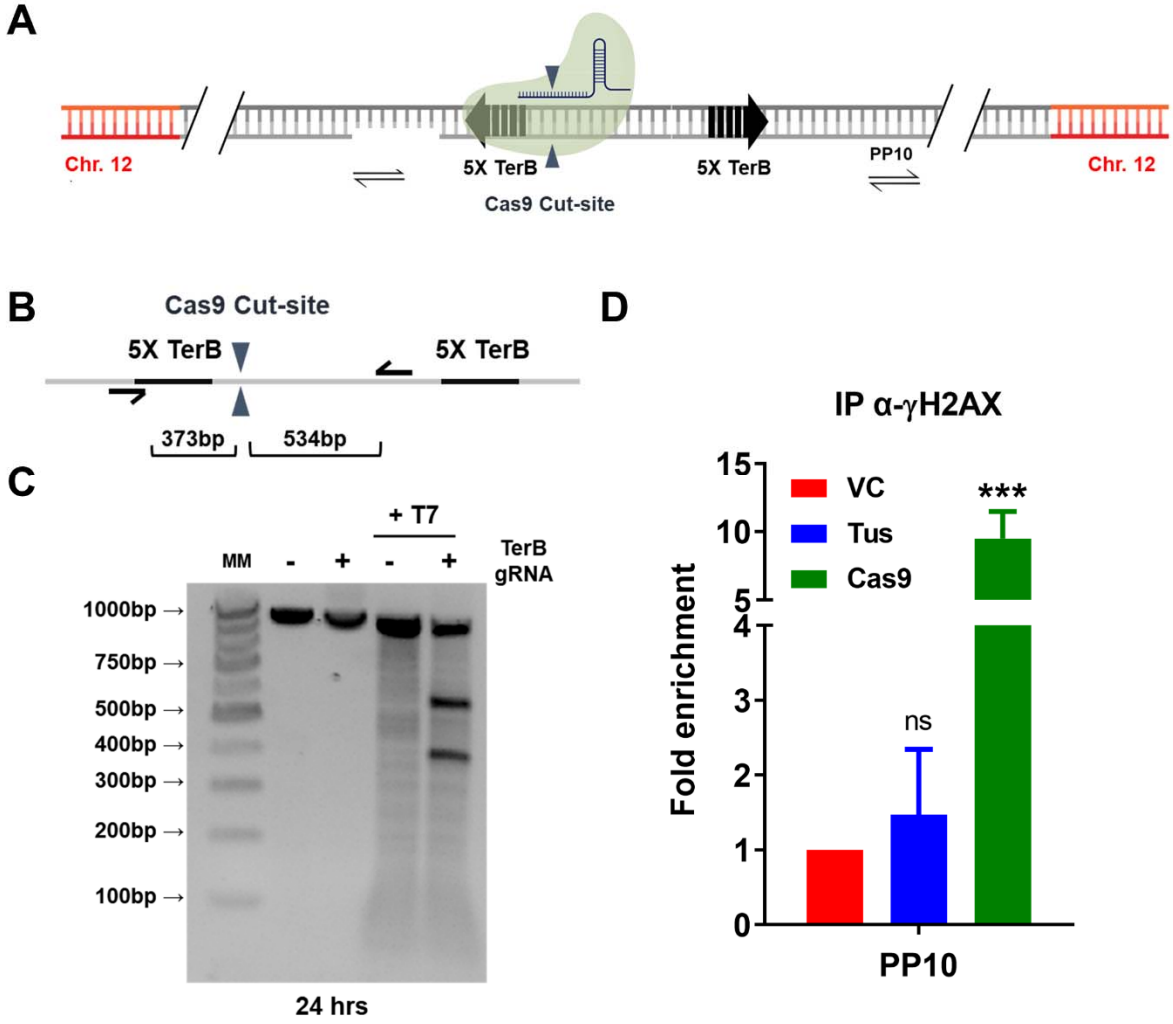

Supplementary Figure 4. **Distinct patterns of γH2AX enrichment at a Cas9-mediated DSB vs the Tus-*TerB* fork barrier: (A)** Schematic of the linearized *TerB* plasmid (pWB15) integrated as a unique copy into MCF7 cells (MCF7 5C-TerB) with the Cas9-binding site (green protein). Blue triangles: Cas9 cut site. Black half-arrow heads depict PCR products expected from primer pair (PP10) used in quantitative PCR (qPCR) are shown. **(B)** Schematic depicting the Cas9 cut site (blue arrows), site-specific PCR primers (black half-arrowhead) and predicted size of cleavage products. **(C)** PCR analysis by T7 assay of MCF7 5C-TerB cells transfected with Cas9-sgRNA RNP complex. **(D)** γH2AX levels along the integrated *TerB* plasmid were analyzed by ChIP-qPCR in MCF7 5C-TerB cells transfected with VC, Tus or Cas9 expression

815 plasmids using the indicated primer pair. Data shows the fold enrichment relative to IgG
816 controls (n=2).

817

Sup Figure 5.

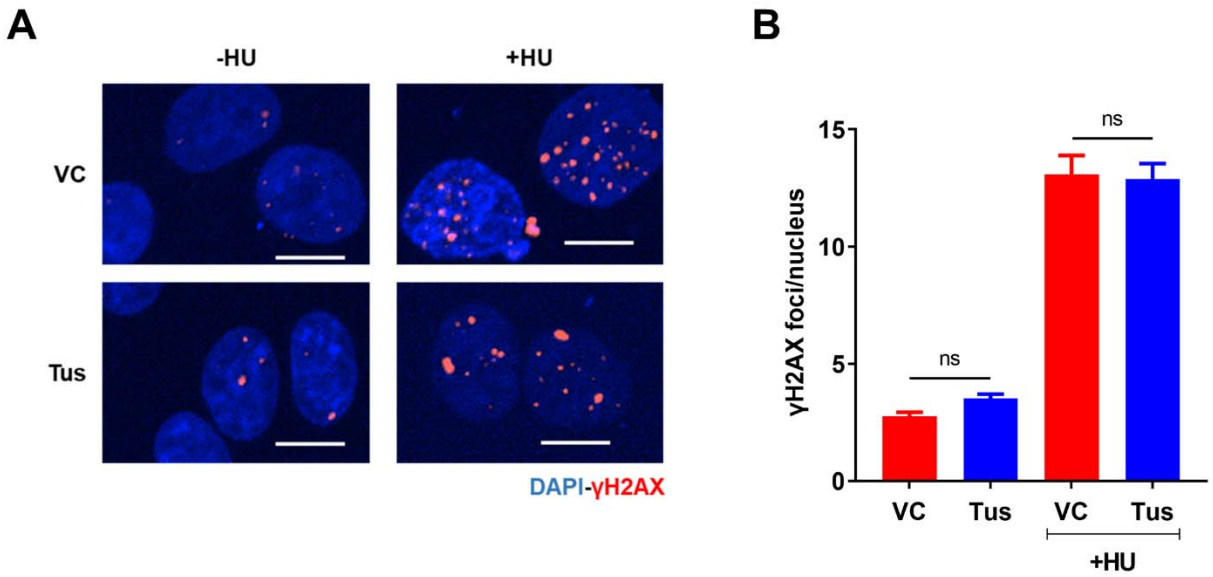

818

819 **Supplementary Figure 5. Genome-wide gH2AX foci were unaffected with Tus**
820 **expression. (A)** Representative images of gH2AX foci across stated conditions. Bars,
821 10 µm **(B)** Average number of gH2AX foci per nucleus in conditions stated. Cells treated
822 with or without 2mM HU for 4 hours. (n=3, ≥300 cells per experiment)

823

Sup Figure 6.

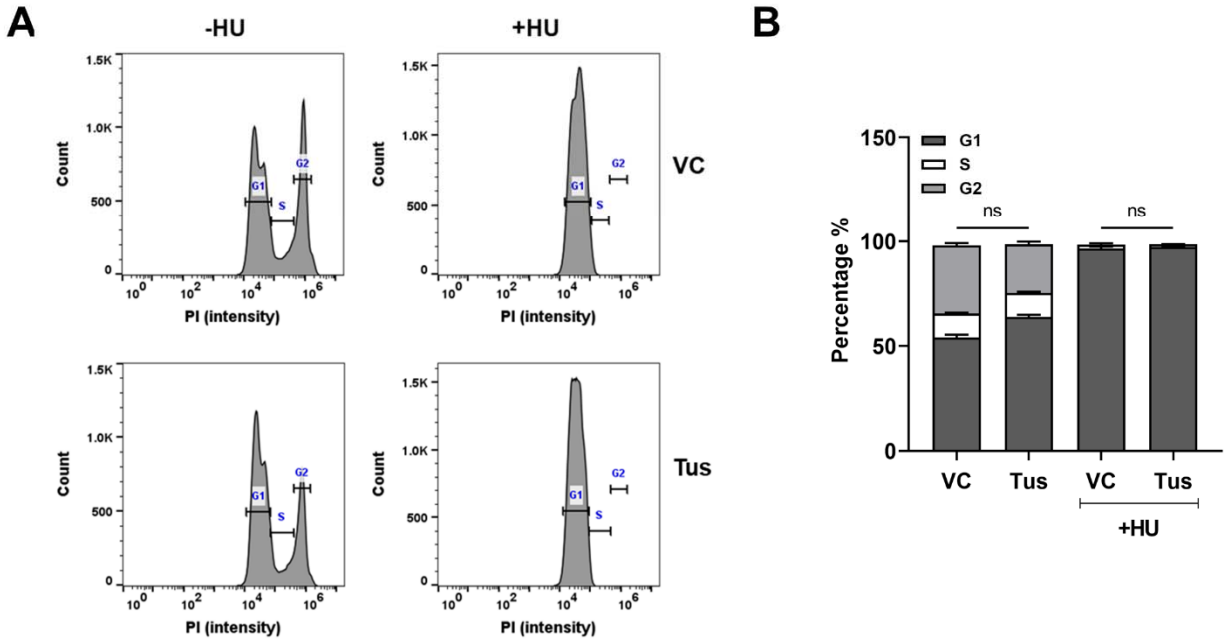

824

825 **Supplementary Figure 6. Cell cycle progression were unaffected with Tus**
826 **expression. (A)** Cell cycle analysis and **(B)** quantification was performed using flow
827 cytometry following staining with propidium iodide staining in MCF7 5C-TerB cells under
828 the stated conditions. Cells treated with or without 2mM HU for 4 hours. (n=3, ns: non-
829 significant)

830

831 ## Supplementary Tables

832 **Supplementary Table 1. Demonstration that the Tus-Ter replication fork block**
833 **does not activate significant replication elsewhere in the genome.** Replication
834 characteristics of 200 kb global DNA segments that represent the total genome. These
835 measurements do not include the segments containing the *TerB* sequence. The table
836 compares MCF7 cells containing the *TerB* sequence with and without Tus induced. This
837 was determined on stretched DNA molecules that had completely incorporated IdU,
838 CldU or a combination of both nucleotide analogues.

839 **Supplementary Table 2. List of antibodies, oligos and plasmids used in the study**.